Published in final edited form as:

Biochemistry. 2018 July 17; 57(28): 4155–4164. doi:10.1021/acs.biochem.8b00415.

Biophysical Examination of the Calcium-Modulated Nickel-Binding Properties of Human Calprotectin Reveals Conformational Change in the EF-Hand Domains and His_3Asp Site

Toshiki G. Nakashige[1], **Sarah E. J. Bowman**[1,2,3,4], **Emily M. Zygiel**[1], **Catherine L. Drennan**[1,2,3,*], and **Elizabeth M. Nolan**[1,*]

[1]Department of Chemistry, Massachusetts Institute of Technology, Cambridge, MA 02139, USA

[2]Department of Biology, Massachusetts Institute of Technology, Cambridge, MA 02139, USA

[3]Howard Hughes Medical Institute, Massachusetts Institute of Technology, Cambridge, MA 02139, USA

Abstract

Calprotectin (CP, S100A8/S100A9 oligomer, MRP-8/MRP-14 oligomer) is a host-defense protein that sequesters nutrient transition metals from microbes. Each S100A8/S100A9 heterodimer contains four EF-hand domains and two transition-metal-binding sites. We investigate the effect of Ca(II) ions on the structure and Ni(II)-binding properties of human CP. By employing energy dispersive X-ray (EDX) spectroscopy, we evaluate the metal content of Ni(II)-bound CP-Ser (oligomer of S100A8(C42S) and S100A9(C3S)) crystals obtained in the absence and presence of Ca(II). We present a 2.1-Å resolution crystal structure of Ni(II)-bound CP-Ser and compare this structure to a reported Ni(II)- and Ca(II)-bound CP-Ser structure (Nakashige, T. G. *et al. J. Am. Chem. Soc.* **2017**, *139*, 8828–8836). This analysis reveals conformational changes associated with Ca(II) coordination to the EF-hands of S100A9, and that Ca(II) binding affects the coordination number and geometry of the Ni(II) ion bound to the His_3Asp site. In contrast, negligible differences are observed for the Ni(II)-His_6 site in the absence and presence of Ca(II). Biochemical studies show that, whereas the His_6 site has a thermodynamic preference for Ni(II) over Zn(II), the His_3Asp site selects for Zn(II) over Ni(II), and relatively rapid metal exchange occurs at this site. These observations inform the working model for how CP withholds nutrient metals in the extracellular space.

Graphical Abstract

[*]Corresponding authors: cdrennan@mit.edu and lnolan@mit.edu Phone: 617-452-2495.
[4]Current address: Hauptman-Woodward Medical Research Institute, Buffalo, NY 14203, USA

Supporting Information
Complete experimental methods, Tables S1–S8, Figures S1–S7, and supporting references. This material is available free of charge via the Internet at http://pubs.acs.org.

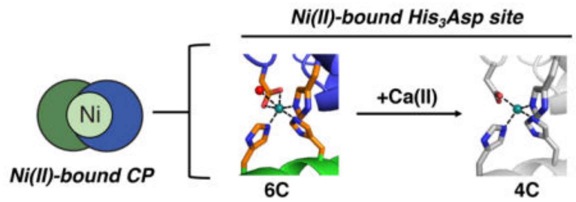

Introduction

Calprotectin (CP, S100A8/S100A9 oligomer, MRP-8/MRP-14 oligomer) is an abundant metal-chelating protein that is released at sites of microbial infection as part of the host innate immune response.[1–5] CP exhibits broad-spectrum antimicrobial activity attributed to its ability to sequester essential metal nutrients from invading pathogens.[1,4,6,7] Human CP coordinates divalent first-row transition metals, including Mn(II),[8–13] Fe(II),[14–16] Ni(II),[17] Cu(II),[18] and Zn(II),[8,19,20] with sufficiently high affinity to prevent microbial acquisition of these nutrients.

CP is the heterooligomer of the S100 proteins S100A8 (α subunit) and S100A9 (β subunit).[21,22] The CP heterodimer exhibits six different sites for coordinating metal ions. Each subunit has two Ca(II)-binding EF-hand domains, a C-terminal canonical ("calmodulin-like") site and an N-terminal non-canonical site.[23–25] Apo CP exists as the αβ heterodimer, and Ca(II) coordination at the EF-hand domains causes two heterodimers to self-associate and form the $\alpha_2\beta_2$ heterotetramer.[22,23,26,27] Ca(II) binding also increases the transition-metal affinities of CP,[9,14,19] enhances its antimicrobial activity,[2,4,19] and affords greater proteolytic stability.[28] The two transition-metal sites are present at the interface between the S100A8 and S100A9 subunits. The His_3Asp motif (site 1) is composed of (A8)His83, (A8)His87, (A9)His20, and (A9)Asp30. This site coordinates Zn(II) with high affinity such that it can sequester Zn(II) from microbes.[14,20] It also coordinates Mn(II),[9] Fe(II),[15] and Ni(II).[17] The His_6 site (site 2) is composed of (A8)His17, (A8)His27, (A9)His91, (A9)His95, (A9)His103, and (A9)His105. This site is functionally versatile because it has the capacity to sequester multiple first-row transition metal ions from microbes. Site 2 coordinates Mn(II),[10–12] Fe(II),[14,15] Ni(II),[17] and Zn(II)[20] in an octahedral environment with relative affinities that agree with the Irving-Williams series ($K_{d,Mn} > K_{d,Fe} > K_{d,Zn} > K_{d,Ni}$).[9,14,17,29]

Despite multiple reports demonstrating that Ca(II) affects the structural and functional properties of CP, we currently have a limited molecular understanding of these processes. For proteins that exhibit Ca(II)-dependent conformational changes such as calmodulin, X-ray crystallography has been instrumental in understanding structural flexibility in the absence and presence of Ca(II).[30] This technique has also yielded four structures of CP to date: one structure of Ca(II)-bound CP (PDB: 1XK4),[23] two structures of Mn(II)- and Ca(II)-bound CP (PDB: 4GGF, 4XJK),[10,12] and a structure of Ni(II)- and Ca(II)-bound CP (PDB: 5W1F).[17] These studies have provided invaluable insights into the coordination chemistry of this host-defense protein and a guide for many studies. Nevertheless, all reported crystal structures of CP are of Ca(II)-bound forms and thus provide no insight into

Ca(II)-free forms of the protein as well as how Ca(II) binding affects protein structure, the transition metal sites, and ultimately function.

In this work, we report crystallographic and solution studies of Ni(II) binding to human CP in the absence and presence of Ca(II). We first employ a single-crystal elemental analysis synchrotron technique to evaluate the metal content of X-ray quality crystals of CP obtained in the presence of Ni(II) ions only or both Ni(II) and Ca(II) ions. Moreover, we present an X-ray structure of Ni(II)-bound CP and compare this structure to a reported Ni(II)- and Ca(II)-bound CP structure.[17] This analysis highlights conformational changes that occur at the EF-hand domains of S100A9 with Ca(II) binding, as well as a change in the Ni(II) coordination number of site 1. In contrast, the Ni(II)-His_6 motif at site 2 undergoes negligible structural change as a result of Ca(II) binding. Although the presence of Ca(II) ions affect the Ni(II) coordination spheres at site 1 and site 2 differently, solution studies show that Ca(II) ions enhance the Ni(II) affinities of both sites. Lastly, a comparison of metal substitution at the His_3Asp and His_6 sites shows markedly different behavior. Whereas the His_6 site entraps and retains a bound metal ion, the His_3Asp site rapidly selects for Zn(II). Taken together, this work informs how Ca(II) ions modulate transition metal binding by CP and, in particular, provides new insight into metal chelation by the His_3Asp motif.

Experimental Methods

Complete experimental methods are provided as Supporting Information.

Results

Metal Analysis of Single Crystals by Energy Dispersive X-ray Spectroscopy

Previous crystallographic studies employed CP-Ser,[10,12,17,23] the heterooligomer of S100A8(C42S) and S100A9(C3S) (Table S1), to avoid disulfide bond formation, and we use this variant in the current study. These two Cys residues are not implicated in transition-metal binding, and CP-Ser exhibits comparable metal-binding properites and antimicrobial activity to native CP.[19] Purified CP-Ser is purified without use of an affinity tag, and following column chromatography, the protein is dialyzed against Chelex resin to reduce metal contamination.[19] We obtained crystals of Ni(II)-bound CP-Ser employing the sitting-drop vapor diffusion method, using a 1:1 molar ratio of Ni(II) and CP-Ser heterodimer. The precipitant solution of 200 mM Li_2SO_4, 100 mM Tris, 20% (v/v) PEG 3350, pH 8.0 did not include added Ca(II) ions. Because Ca(II) ions are a common contaminant, we sought to compare the Ca(II)-free and Ca(II)-bound forms of Ni(II)-bound CP-Ser and employed energy dispersive X-ray (EDX) spectroscopy to evaluate the levels of calcium and other metals in the crystals (Figure 1). Based on an established method to evaluate the elemental composition of materials,[31] this technique can be utilized to analyze the X-ray fluorescence of elements present in single-crystal samples and can be used in tandem with collecting diffraction data on the synchrotron beamline.[32] X-rays at a fixed incident energy are used to excite elements that emit photons corresponding their K-edge energies, with Compton backscattering observed near the incident energy. Fluorescence counts of various elements are detected, and emission spectra are calibrated to a standard containing Sm, Ni, Zn, Br, and Sr. Crystals were analyzed on 100-μm loops, and measurements for the sample (X-rays positioned on crystal, red lines in Figure 1) and a blank (X-rays positioned on an empty space of the loop, black lines in Figure 1) were taken at 0.9792 Å incident energy. Data acquisition times were the same for each pair of sample and blank.

Results from this single-crystal elemental analysis indicate that the crystal obtained in the absence of Ca(II) and later employed for X-ray diffraction (*vide infra*) contained negligible Ca ($K\alpha_1$ 3.69 keV) compared to the blank (Figure 1A,1C). In contrast, the Ca content was notably higher for a crystal obtained under the same crystallization conditions that was subsequently soaked in Ca(II) (i.e., Ni(II)- and Ca(II)-bound CP-Ser described previously[17]) (Figure 1B,1C). We also employed EDX line scans to evaluate relative concentrations of transition metals, including Ni and contaminants that could be present in the crystallization conditions. Both crystals exhibited high concentrations of Ni ($K\alpha_1$ 7.48 keV, $K\beta_1$ 8.26 keV). In addition, contaminating levels of Zn ($K\alpha_1$ 8.64 keV) and trace amounts of Fe ($K\alpha_1$ 6.40 keV) were detected. Nevertheless, we expect that Ni will be in excess of any contaminating metal ions, and this elemental analysis in conjunction with our anomalous scattering data (*vide infra*) supports (i) that the Ni(II)-bound crystal is effectively Ca(II)-free and (ii) that Ni(II) ions can be unambiguously assigned to the transition-metal-binding sites.

Crystal Structure of Ni(II)-bound CP-Ser in the Absence of Ca(II)

X-ray diffraction data were collected on the Ni(II)-containing crystal obtained in the absence of added Ca(II) that was analyzed by EDX spectroscopy, and a structure was solved to 2.1-Å resolution (Table S2) by employing the Mn(II)-, Ca(II)-, and Na(I)-bound CP-Ser crystal structure (PDB: 4XJK)[12] as the molecular replacement model. Ni(II)-bound CP-Ser crystallized as an $\alpha_2\beta_2$ heterotetramer (Figure 2A).

Electron density at the four transition-metal-binding sites of the tetramer was consistent with metals bound at one of the His_3Asp motifs and both His_6 motifs of the tetramer (Figure 2B, Tables 1, S3–S6). To confirm the identity of the metals at these sites, anomalous scattering datasets were also collected at the Ni (1.4831 Å) and Fe (1.7370 Å) K-edges and processed to 2.3- and 2.6-Å resolution, respectively. Maps generated from these anomalous data support that all three metal ions are Ni(II). Anomalous signal is observed at the Ni peak (Figure 2B), and we assigned Ni(II) ions at 100% occupancy at all three sites (Table 1). Thus, although the crystallization conditions contained only 1.0 equiv Ni(II) relative to the heterodimer, the crystallization yielded a 3:2 Ni(II) to CP heterotetramer ratio. This same ratio was observed in the structure of Ni(II)- and Ca(II)-bound CP-Ser that contains Ni(II) ions bound to both His_6 sites and one His_3Asp site of the heterotetramer, suggesting that the metallation state of CP-Ser is not homogeneous under crystallization conditions and that the more fully metallated protein is preferentially crystallized.[17]

The EDX data (*vide supra*) show no Ca signal in Ni(II)-bound CP-Ser crystals and anomalous maps generated using data collected at the Fe K-edge (1.7370 Å) also indicate a lack of Ca(II) ions (Figure S1). Because the Ca K-edge at 3.3582 Å is inaccessible for data collection at most synchrotrons, Ca(II) scattering is often evaluated by using data collected at the Fe Kedge (1.7370 Å). The Fe anomalous maps show density for the Ni(II) ions that are bound at sites 1 and 2, as expected, because Ni scatters anomalously at this wavelength. Ca, if present in the sample, should display stronger anomalous scattering than Ni at the Fe

K-edge wavelength, but no anomalous density is present at the EF-hand domains (Figure S1), suggesting that Ca(II) is not bound. To determine if another atom is bound in these sites, the electron density was evaluated. Three of the eight EF-hands do not exhibit electron density, and we consider these sites to be metal-free (Table 1). The other five EF-hand domains exhibit electron density consistent with an atom present at these sites. Previous structures have been refined with Na(I) ions at select EF-hands,[12,17] and our crystallization condition contained 1000-fold excess Na(I) (100 mM) compared to the concentration of CP-Ser (100 μM). To evaluate if Na(I) ions provide a good fit in this structure, Na(I) was refined at 100% occupancy in all five sites (Tables 1, S7). No positive or negative difference electron density appeared, indicating that Na(I) is consistent with the crystallographic data.

Conformational Changes at the EF-hand Domains upon Ca(II) Coordination

To examine the conformational changes that occur upon Ca(II) coordination, we compared the Ni(II)-bound CP-Ser structures obtained in the absence and presence of Ca(II). We first examined the EF-hand domains of S100A9 that are adjacent to site 1 (Figure 3). Dimer 1 has no metal at the His_3Asp motif (site 1) in both structures, and the Ca(II)-free species (Figure 3A), in which both EF-hand domains are empty, exhibits several sidechain and loop rearrangements when compared to the Ca(II)-bound structure (Figure 3B). In particular, the loop that contributes (A9)Asp30 has undergone a conformational rearrangement, resulting in substantially different positions for (A9)Leu26 and (A9)His28 and an altered conformation of the (A9)Asp30 residue that is pointing away from the three His residues of the His_3Asp motif ((A9)His20, (A8)His83, (A8)His87 in Figure 3A). With the non-canonical site empty in the Ca(II)-free structure, the side chain of (A8)His87 of the His_3Asp motif has also moved toward the empty site, and (A9)His20 of the His_3Asp motif has moved down toward the position vacated by (A8)His87 (Figure 3A). The net result of these movements is that three of the four residues of the His_3Asp motif are not arranged to bind a metal ion. Site 1 is also empty in the Ca(II)-bound structure (Figure 3B), but the side chains of all the residues of the His_3Asp motif are all much closer to their metal-binding orientations (compare Figure 3B to Figure 3D). In the Ca(II)-bound structure, Na(I) occupies the non-canonical site, which further stabilizes the (A9)Asp30 loop and helps to maintain the positions of (A8)His87 and (A9)His20 in their metal-binding orientations (Figure 3B). Connectivity in dimer 1 between the canonical EF-hand with Ca(II) bound, the non-canonical site with Na(I) bound, and site 1 is apparent in the Ca(II)-bound structure (Figure 3B). In particular, residues of the S100A9 canonical EF-hand (i.e., Asp67, Asn69, Asp71, Gln73, and Glu78) adjust upon Ca(II) binding and Gln73 moves closer to the non-canonical site where it forms a hydrogen bond to a coordinating water of the bound Na(I) ion, the non-canonical site appears to be stabilized, and the resulting well-ordered non-canonical site appears to stabilize residues of the His_3Asp motif in metal-binding orientations (Figure 3B).

Although dimer 2 displays fewer conformational rearrangements between the Ca(II)-bound and Ca(II)-free structures, the same general trends as described above are observed. Dimer 2 coordinates a Ni(II) ion in the His_3Asp motif (site 1) in both structures, and both structures have a metal ion, either Na(I) or Ca(II), in the non-canonical site (Figure 3C,D). As observed in dimer 1, ordering of EF-hand residues upon Ca(II) binding results in the formation of a hydrogen bond between (A9)Gln73 and a water molecule that is coordinated to the metal in the non-canonical site, and the non-canonical site is well-ordered and residues of the His_3Asp motif are positioned to bind Ni(II) (Figure 3D). In the Ca(II)-free structure, (A9)Gln73 does not hydrogen bond to the Na(I)-coordinating water, and Na(I) has fewer protein ligands than are observed at this dimer 2 site when Ca(II) is bound. Namely, Na(I) has two sites occupied by water molecules in the Ca(II)-free structure whereas the Ca(II) ion at the non-canonical site is coordinated by (A9)Glu36 in a bidentate fashion. Importantly, neither Ni(II)-bound CP-Ser structure includes a CP heterodimer species with a Ni(II) ion at site 1 and without a metal ion at the S100A9 non-canonical EF-hand (i.e., site 1 is not occupied unless a metal is present at the non-canonical EF-hand), which suggests that cooperativity exists between these two sites. Lastly, although a Ni(II) ion is bound at site 1 of dimer 2 in the absence of Ca(II), the geometry and ligand identity is altered (*vide infra*).

The Ni(II) Coordination Sphere at the His_3Asp Motif

The conformational changes of the EF-hand domains adjacent to site 1 of dimer 2 result in a shift in the primary coordination sphere of Ni(II) at the His_3Asp motif (Figure 4 and Supporting Video). The Ca(II)-free CP-Ser structure exhibits a six-coordinate Ni(II) center, where the bond distances and angles are consistent with a pseudooctahedral coordination environment (Tables S3, S4). In addition to the three His residues, a bidentate (A9)Asp30, and a solvent-derived water molecule complete this site. When Ca(II) binds at the adjacent S100A8 EF-hand domains, Asp30 rotates ≈45°, positioning one of the oxygen ligands (Oδ2) ≈0.5 Å away from the Ni(II) ion, thereby forming a tetrahedral Ni(II) center with a monodentate (A9)Asp30 and no coordinating water molecule. Thus, although Ni(II) can bind to site 1 without Ca(II) being present, only the Ca(II)-bound structure displays the tetrahedral His_3Asp arrangement that is associated with higher affinity metal binding.

The Ni(II) Coordination Sphere at the His_6 Motif

Site 2 is adjacent to the EF-hand domains of S100A8 (Figure S2). However, structural alignments show that site 2 does not exhibit marked conformational changes upon Ca(II) binding to the S100A8 EF-hand domains (Figures 5, S2). In the Ca(II)-free structure, Na(I) ions are present at both EF-hand domains, and in the Ca(II)-bound structure, Ca(II) replaces Na(I) at the canonical EF-hand. Regardless of identity, the primary coordination sphere of the metal bound to the S100A8 EF-hand domain is the same. Moreover, the Ni(II)-bound His_6 motifs are nearly identical in the absence or presence of Ca(II) (Figure 5), and atoms comprising the His_6 motifs harbor similar B-factors for both the Ca(II)-free and Ca(II)-bound structures, indicating that these sites have comparable degrees of order. Thus, the Ca(II)-free structure does not provide information into how Ca(II) influences the metal-binding affinity at site 2, and further investigations are required to probe this phenomenon.

Ni(II) Coordination Causes Tetramerization in Solution

To complement crystallographic analyses and further our understanding of how Ni(II) binding affects the biophysical properties of CP-Ser in solution, we performed solution studies to examine Ni(II) binding in the absence and presence of Ca(II) ions. We first employed analytical size-exclusion chromatography (SEC) to examine the effect of Ni(II) coordination on the quaternary structure of CP-Ser and protein variants. The variants lack residues of site 1 (ΔHis_3Asp), site 2 (ΔHis_4), or both sites 1 and 2 ($\Delta\Delta$) or His residues of the S100A9 C-terminal tail (AAA, AHA, H103A, H104A, H105A) (Table S1).

All apo CP variants exhibit peak elution volumes of ≈11.4 mL, consistent with the presence of αβ heterodimers (Figure S3).[19] Following preincubation of CP-Ser, ΔHis_3Asp, and H104A with 5 equiv of Ni(II), the peak elution volumes shifted to ≈10.8 mL. These new peaks exhibit comparable elution volumes to that of the Ca(II)-bound $\alpha_2\beta_2$ heterotetramer, indicating formation of Ni(II)-bound $\alpha_2\beta_2$ heterotetramers in the absence of Ca(II). In contrast, when ΔHis_4 and $\Delta\Delta$ were preincubated with 5 equiv of Ni(II), the proteins exhibited the same peak elution volume as apo CP-Ser. Thus, these two variants did not form heterotetramers as a result of Ni(II) preincubation. We previously determined the stoichiometry of Ni(II) binding to CP-Ser and variants by SEC and observed that CP-Ser retained ≈2 equiv of Ni(II) and that ΔHis_3Asp and ΔHis_4 retained ≈1 equiv of Ni(II) over the elution protocol.[17] These data indicate that Ni(II) binding at site 2, and not at site 1, results in tetramerization. This observation is consistent with prior studies that show that coordination of Mn(II) or Fe(II) to the His_6 site of CP-Ser results in the formation of a Ca(II)-free heterotetramer.[28] Lastly, whereas the AHA, H103A, and H105A variants exhibit comparable elution volume peak shifts with Ni(II) to CP-Ser, the AAA variant appears to have perturbed tetramerization because its chromatogram displays a shoulder. Similar behavior was observed for Mn(II) binding to the tail variants, where the presence of the His residues in the S100A9 C-terminal tail are important for complete transformation to the heterotetrameric species.[11]

Ni(II) Coordination Increases the Thermal Stability of CP

On the basis of our prior studies of Mn(II) and Zn(II) chelation to CP-Ser,[9,19] we expected that Ni(II) binding enhances the thermal stability of the protein. We employed circular dichroism (CD) spectroscopy to monitor the thermal denaturation of CP-Ser in the presence of Ni(II) and both Ni(II) and Ca(II) (Figure S4). In the absence of Ca(II), Ni(II) binding increases the melting temperature (T_m) of CP-Ser from ≈65 °C to ≈80 °C. In the presence of both Ni(II) and Ca(II), negligible protein unfolding was observed until >95 °C. These trends are consistent with results from prior thermal denaturation studies of Zn(II) and Mn(II) coordination.[9,19]

Ca(II) Ions Enhance the Ni(II) Affinity of CP

Our prior studies indicated that Ca(II) enhances the ability of CP to deplete Ni from bacterial growth media.[14] We therefore reasoned that the affinity of CP for Ni(II) depends on Ca(II) coordination, as observed for other transition metals.[9,14,19] We conducted Ni(II) competition experiments employing the Ca(II)-insensitive metal sensor Zinpyr-1 (ZP1), which displays fluorescence quenching as a result of Ni(II) complexation (Figure S5).[33] Although we did not ascertain an apparent dissociation constant value of ZP1 for Ni(II) and thus quantitative assessment of Ni(II) affinities for CP-Ser, this study indicated that Ca(II) ions enhance the Ni(II) affinity of CP-Ser (Figure S6). When Ni(II) was added to equimolar mixtures of ZP1 and CP-Ser in the absence and presence of excess Ca(II) ions, the fluorescence from ZP1 indicated that most of the added Ni(II) is bound to CP-Ser under both conditions, and that a larger fraction of total Ni(II) is bound to CP-Ser in the presence of Ca(II).

Ca(II) Coordination Results in Slower Exchange of Zn(II) for Ni(II) at the His_6 Site

We previously observed that the presence of Ca(II) caused the substitution for transition metals (e.g. Mn(II), Fe(II), Zn(II)) at the His_6 site to occur relatively slowly.[14] To extend this work to Ni(II), we conducted a metal-substitution assay where we monitored the exchange of Ni(II) and Zn(II) at site 2 in the absence and presence of Ca(II) over 72 h (Figure 6). We pre-incubated B-ΔHis_3Asp, a biotinylated ΔHis_3Asp variant (Table S1),[17] with 1.0 equiv of either Ni(II) or Zn(II) and then added 1.0 equiv of the other metal ion. We then performed pull-down with streptavidin resin at varying time points and quantified the metal content in the resulting supernatant by inductively coupled plasma-mass spectrometry (ICP-MS). At the end of each time course, a higher concentration of Zn(II) remained in the supernatant, suggesting that B-ΔHis_3Asp removed during the pull-down step was predominately the Ni(II)-bound species. When Ni(II) was added first, Zn(II) displaced ≈30% of the Ni(II) over the incubation period (Figure 6A). When Zn(II) was added first, Ni(II) displaced ≈70% of the Zn(II) (Figure 6B). Thus, site 2 has a thermodynamic preference for Ni(II) over Zn(II) in the presence and absence of Ca(II), and the exchange between these two metal ions occurs more slowly in the presence of Ca(II).

The His_3Asp Site Selects for Zn(II) Over Ni(II)

Since the discovery that site 2 is a biologically unprecedented His_6 site that sequesters Mn(II) and other metal ions, many studies have focused on delineating its biophysical and functional properties, and less emphasis has been placed on characterizing the His_3Asp site.[10–12,14–17,20] Nevertheless, investigations of CP-Ser[20] as well as the host-defense proteins S100A7[34] and S100A12[35] have demonstrated that His_3Asp sites sequester Zn(II). Moreover, studies of metal depletion from microbial growth media indicate that His_3Asp sites select for Zn(II) over other metals, including Ni(II).[14,34,35] We therefore sought to examine metal exchange at the His_3Asp site using the pull-down assay described above. Efforts to purify a biotinylated His_4 variant resulted in poor yields because the protein routinely precipitated, and we were unable to readily obtain sufficient quantities of this protein for the assay. We thus optimized a spin-filtration assay to examine metal substitution at the His_3Asp site (Supporting Discussion). Under conditions of excess Ca(II), we pre-loaded 10 μM CP-Ser with 2.0 equiv of Ni(II) and added 1.0 equiv of Zn(II) to the solution (75 mM HEPES, 100 mM NaCl, pH 7.4, 2 mM Ca(II)). Following incubation (up to 120 min), the bound and unbound fractions were separated via spin filtration (10-kDa MWCO membrane), and the filtrate (unbound fraction) was analyzed by ICP-MS. Because site 2 has a thermodynamic preference for Ni(II) over Zn(II) (Figure 6), we reasoned that any unbound Ni(II) that is detected after Zn(II) addition would originate from the His_3Asp site. ICP-MS analysis of samples taken at varying time points after Zn(II) addition revealed that the filtrate contained ≈2 μM Zn(II) and ≈7 μM Ni(II) following 10 min, which is the earliest time point that could be reliably analyzed by this method (Figure 7A). Over the course of 120 min, the concentrations of Zn(II) and Ni(II) in the filtrate further decreased and increased, respectively, indicating that Ni(II) had been displaced from the His_3Asp site by Zn(II). Moreover, a control performed with the ΔHis_3Asp variant showed that Ni(II) remains bound to the His_6 site under the assay conditions (Figure 7B). We also conducted this experiment in the absence of added Ca(II), and we observed similar metal substitution at site 1 of CP-Ser in the absence or presence of Ca(II) (Figure S7). Overall, these results demonstrate that the

His_3Asp site has a thermodynamic preference for Zn(II) over Ni(II) and exhibits markedly more rapid metal exchange kinetics than the His_6 site.

Discussion

In this work, we pursued X-ray protein crystallography and solution experiments to evaluate Ni(II) binding by CP-Ser under conditions of low and high Ca(II) concentrations. This initiative was motivated by our previous report that CP-Ser binds Ni(II) at the His_3Asp and His_6 sites, and sequesters this metal nutrient from *Staphylococcus aureus* and *Klebsiella pneumonaie*, two bacterial pathogens that can colonize the urinary tract and employ the Ni-enzyme urease during urinary tract infections.[17] It also addresses the fundamental and unresolved question of how Ca(II) binding affects the structure and function of this remarkable host-defense protein. In particular, structural comparisons of the Ni(II)-bound CP-Ser structure and our previously reported Ni(II)- and Ca(II)-bound structure reveal conformational changes associated with Ca(II) binding to the EF-hand domains and provide insight into how Ca(II) ions influence transition-metal coordination by CP. This study also examines the metal-exchange properties of the His_3Asp site of CP, which has received less attention than the His_6 site to date.

We first employed EDX spectroscopy to discern the metal content of CP-Ser crystals that we subsequently examined by X-ray diffraction. This synchrotron technique allows high-resolution detection of K-edge energy emission of metals such as Ca, Mn, Fe, Ni, and Zn.[32] Unlike traditional methods for elemental analysis such as ICP-MS and atomic absorption/emission spectroscopy, EDX line scans can be collected on crystalline samples as small as 50 μm in length and can be obtained in tandem with X-ray diffraction experiments. Employing EDX spectroscopy, in combination with anomalous scattering, was helpful in this crystallographic work because CP-Ser has the capacity to coordinate a number of different metal ions. The technique confirmed that negligible Ca was present in the Ca(II)-free crystal and, along with X-ray anomalous data, contributed to our unambiguous assignment of Ni(II) ions at the transition-metal-binding sites.

From the standpoint of biological Ni(II) sites, CP-Ser is unusual because it can exhibit three different Ni(II) coordination motifs. Site 1 (His_3Asp) exhibits one of two coordination modes depending on the presence of Ca(II): (i) a pseudooctahedral Ni(II) site composed of three nitrogen and three oxygen donors when Ca(II) is absent, and (ii) a tetrahedral Ni(II) site composed of three nitrogen donors and one oxygen ligand when Ca(II) is bound. Analysis of Ni(II)-chelating proteins in the Protein Data Bank (PDB)[36] using the MESPEUS online database[37] reveals only one other protein with a metal-binding site that is comparable to the six-coordinate Ni(II) center at site 1 (Table S8). The transcriptional regulator TM1602 of *Thermotoga maritima* has a His_3Glu motif where the bidentate Glu residue and a water molecule complete the Ni(II) coordination sphere.[38] Moreover, to the best of our knowledge, no other four-coordinate Ni(II) site with three His residues and a carboxylate ligand is deposited in the PDB (Table S8). Site 2 is the hexahistidine site, and this Ni(II) motif has previously only been identified for His-tagged or engineered proteins.[39–41] Nevertheless, in small-molecule complexes, mononuclear hexaimidazole Ni(II) centers have been structurally characterized,[42,43] and the Ni(II)-His_6 sites of CP observed in the absence and presence of bound Ca(II) ions exhibit metal–ligand bond lengths comparable to these complexes.

The Ca(II)-induced conformational changes that occur at the His_3Asp motif and the S100A9 EF-hand domains adjacent to site 1 shows a new facet of how transition-metal binding is modulated at site 1, at least in the case of a bound Ni(II) ion. At present, there is a paucity of information about the geometric and electronic structures of M(II)-His_3Asp in CP, and reported studies are limited to Fe(II) and Co(II).[15,19] Comparable optical absorption transitions, suggesting a 4- or 5-coordinate geometry, are observed for Co(II) bound to the His_3Asp site in the absence and presence of Ca(II).[19] Subsequent near-infrared (NIR) magnetic circular dichroism (MCD) spectroscopic studies of Fe(II)-bound CP-Ser revealed a five-coordinate Fe(II) signal associated with site 1 in both the absence and presence of Ca(II) ions.[15] Although the coordination number of the Fe(II) atom did not change, the presence of Ca(II) ions affected the ligand field of site 1. Thus, whether the change of coordination number of Ni(II) bound to site 1 that occurs with Ca(II) binding is specific to this metal or can be generalized to others such as Zn(II) remains to be determined. Moreover, the exclusion of a solvent-derived ligand at site 1 in the presence of Ca(II) is reminiscent of our prior work on the His_6 site, which supports a model in which the S100A9 C-terminal tail precludes access of water molecules to the metal center and thereby contributes to the metal-sequestering function of CP.[12,15]

Structural comparisons of the Ni(II)-bound His_6 motif in the absence and presence of Ca(II) demonstrate that Ca(II) binding at the EF-hand domains has negligible effect on the primary coordination sphere of site 2. These results are congruous with prior spectroscopic studies on Mn(II) and Fe(II) coordination at this site.[12,15] Together, these data indicate that the enhanced affinities for transition metal ions observed at this His_6 site for the Ca(II)-bound heterotetramer cannot be explained by changes in the primary sphere or electronic structure at this site. We expect that further investigations of allostery and Ca(II)-induced tetramerization will inform how Ca(II) coordination enhances the transition-metal affinities of this site.

Deciphering metal selectivity and exchange at sites 1 and 2 also informs the current model for the metal-withholding function of CP. The present work provides further evidence for relatively slow metal exchange at the His_6 site, and supports the notion that presence of Ca(II) ions reduces the metal exchange rate at this site to some degree. These observations further substantiate a model of "functional versatility" where the His_6 site binds and entraps the metal ion it encounters first. In contrast, the current investigation of metal exchange at the His_3Asp site indicates that it has a thermodynamic preference for Zn(II) over Ni(II) and displays relatively rapid substitution of Zn(II) for Ni(II) in both the absence and presence of Ca(II). The His_3Asp site has been described as Zn(II) selective in prior work, and Zn(II) sequestration by site 1 of CP has been shown to inhibit the growth of *Lactobacillus plantarum* and *Candida albicans*.[20] The current data are consistent with this concept. Nevertheless, a recent study indicates that CP sequesters Cu(II) from *C. albicans* and that both sites 1 and 2 bind Cu(II) with high affinity.[18] Whether the His_3Asp site has thermodynamic preference for Zn(II) or Cu(II) is currently unknown and an avenue for future work.

In closing, Ca(II)-dependent properties of S100 proteins have been studied for several decades,[24,44] and evidence for allosteric communication between the Ca(II)-binding EF-hand domains and transition metal sites has also been reported for S100A12 and S100B.[35,45–47] Although evidence for Ca(II) ions modulating the antimicrobial properties of CP emerged almost thirty years ago,[2] only in the past decade have we learned that allosteric communication between the EF-hand domains and transition metal sites contributes to metal-sequestering ability of CP.[9,14,19] Expanding upon these recent studies, this work on Ni(II)-bound CP-Ser provides a structural snapshot of a Ca(II)-free CP species and motivation for future studies that further address how Ca(II) binding modulates its structural and functional properties.

Supplementary Material

Refer to Web version on PubMed Central for supplementary material.

Acknowledgments

We acknowledge the the NSF (CHE-1352132 to E.M.N.), the NIH (R01GM126376 and R01GM118695 to E.M.N., R01GM069857 to C.L.D., F32-GM099257 to S.E.J.B.), the MIT Center for Environmental Health Sciences (NIH Grant P30-ES002109), the MIT Center for Environmental Health Sciences Theron Randolph Gift (E.M.N.), and the National Science Foundation Graduate Research Fellowship Program (T.G.N. and E.M.Z.) for providing financial support. C.L.D. is a Howard Hughes Medical Investigator. This work is based upon research conducted at the Northeastern Collaborative Access Team beamlines, which are funded by the National Institute of General Medical Sciences from the National Institutes of Health (P41 GM103403). The Pilatus 6M detector on beamline 24-ID-C is funded by a NIH-ORIP HEI grant (S10 RR029205). This research used resources of the Advanced Photon Source, a U.S. Department of Energy (DOE) Office of Science User Facility operated for the DOE Office of Science by Argonne National Laboratory under Contract No. DE-AC02-06CH11357. The Biophysical Instrumentation Facility for the Study of Complex Macromolecular Systems is supported by NSF grant 0070319. The ICP-MS instrument is housed in the MIT Center for Environmental Health Sciences Bioanalytical Core, which is supported by NIH grant P30-ES002109. We also thank Dr. K. Rajashankar for assistance with EDX data analysis, and Dr. E. C. Wittenborn and Ms. T. A. J. Grell for assistance with X-ray diffraction data collection and analysis.

References

1. Sohnle PG, Collins-Lech C, Wiessner JH. The zinc-reversible antimicrobial activity of neutrophil lysates and abscess fluid supernatants. J Infect Dis. 1991; 164:137–142. [PubMed: 2056200]
2. Sohnle PG, Collinslech C, Wiessner JH. Antimicrobial activity of an abundant calciumbinding protein in the cytoplasm of human neutrophils. J Infect Dis. 1991; 163:187–192. [PubMed: 1984467]
3. Johne B, Fagerhol MK, Lyberg T, Prydz H, Brandtzaeg P, Naess-Andresen CF, Dale I. Functional and clinical aspects of the myelomonocyte protein calprotectin. J Clin Pathol: Mol Pathol. 1997; 50:113–123.
4. Corbin BD, Seeley EH, Raab A, Feldmann J, Miller MR, Torres VJ, Anderson KL, Dattilo BM, Dunman PM, Gerads R, Caprioli RM, Nacken W, Chazin WJ, Skaar EP. Metal chelation and inhibition of bacterial growth in tissue abscesses. Science. 2008; 319:962–965. [PubMed: 18276893]
5. Hood MI, Skaar EP. Nutritional immunity: transition metals at the pathogen–host interface. Nat Rev Microbiol. 2012; 10:525–537. [PubMed: 22796883]
6. Clohessy PA, Golden BE. Calprotectin-mediated zinc chelation as a biostatic mechanism in host defence. Scand J Immunol. 1995; 42:551–556. [PubMed: 7481561]
7. Loomans HJ, Hahn BL, Li QQ, Phadnis SH, Sohnle PG. Histidine-based zinc-binding sequences and the antimicrobial activity of calprotectin. J Infect Dis. 1998; 177:812–814. [PubMed: 9498472]
8. Kehl-Fie TE, Chitayat S, Hood MI, Damo S, Restrepo N, Garcia C, Munro Kim A, Chazin Walter J, Skaar Eric P. Nutrient metal sequestration by calprotectin inhibits bacterial superoxide defense

enhancing neutrophil killing of *Staphylococcus aureus*. Cell Host Microbe. 2011; 10:158–164. [PubMed: 21843872]

9. Hayden JA, Brophy MB, Cunden LS, Nolan EM. High-affinity manganese coordination by human calprotectin is calcium-dependent and requires the histidine-rich site formed at the dimer interface. J Am Chem Soc. 2013; 135:775–787. [PubMed: 23276281]
10. Damo SM, Kehl-Fie TE, Sugitani N, Holt ME, Rathi S, Murphy WJ, Zhang Y, Betz C, Hench L, Fritz G, Skaar EP, Chazin WJ. Molecular basis for manganese sequestration by calprotectin and roles in the innate immune response to invading bacterial pathogens. Proc Natl Acad Sci US A. 2013; 110:3841–3846.
11. Brophy MB, Nakashige TG, Gaillard A, Nolan EM. Contributions of the S100A9 C-terminal tail to high-affinity Mn(II) chelation by the host-defense protein human calprotectin. J Am Chem Soc. 2013; 135:17804–17817. [PubMed: 24245608]
12. Gagnon DM, Brophy MB, Bowman SEJ, Stich TA, Drennan CL, Britt RD, Nolan EM. Manganese binding properties of human calprotectin under conditions of high and low calcium: X-ray crystallographic and advanced electron paramagnetic resonance spectroscopic analysis. J Am Chem Soc. 2015; 137:3004–3016. [PubMed: 25597447]
13. Hadley RC, Gagnon DM, Brophy MB, Gu Y, Nakashige TG, Britt RD, Nolan EM. Biochemical and spectroscopic observation of Mn(II) sequestration from bacterial Mn(II) transport machinery by calprotectin. J Am Chem Soc. 2018; 140:110–113. [PubMed: 29211955]
14. Nakashige TG, Zhang B, Krebs C, Nolan EM. Human calprotectin is an iron-sequestering host-defense protein. Nat Chem Biol. 2015; 11:765–771. [PubMed: 26302479]
15. Baker TM, Nakashige TG, Nolan EM, Neidig ML. Magnetic circular dichroism studies of iron(II) binding to human calprotectin. Chem Sci. 2017; 8:1369–1377. [PubMed: 28451278]
16. Nakashige TG, Nolan EM. Human calprotectin affects the redox speciation of iron. Metallomics. 2017; 9:1086–1095. [PubMed: 28561859]
17. Nakashige TG, Zygiel EM, Drennan CL, Nolan EM. Nickel sequestration by the host-defense protein human calprotectin. J Am Chem Soc. 2017; 139:8828–8836. [PubMed: 28573847]
18. Besold AN, Gilston BA, Radin JN, Ramsoomair C, Culbertson EM, Li CX, Cormack BP, Chazin WJ, Kehl-Fie TE, Culotta VC. The role of calprotectin in withholding zinc and copper from *Candida albicans*. Infect Immun. 2018; doi: 10.1120/IAI.00779-00717
19. Brophy MB, Hayden JA, Nolan EM. Calcium ion gradients modulate the zinc affinity and antibacterial activity of human calprotectin. J Am Chem Soc. 2012; 134:18089–18100. [PubMed: 23082970]
20. Nakashige TG, Stephan JR, Cunden LS, Brophy MB, Wommack AJ, Keegan BC, Shearer JM, Nolan EM. The hexahistidine motif of host-defense protein human calprotectin contributes to zinc withholding and its functional versatility. J Am Chem Soc. 2016; 138:12243–12251. [PubMed: 27541598]
21. Hunter MJ, Chazin WJ. High level expression and dimer characterization of the S100 EF-hand proteins, migration inhibitory factor-related proteins 8 and 14. J Biol Chem. 1998; 273:12427–12435. [PubMed: 9575199]
22. Vogl T, Roth J, Sorg C, Hillenkamp F, Strupat K. Calcium-induced noncovalently linked tetramers of MRP8 and MRP14 detected by ultraviolet matrix-assisted laser desorption/ionization mass spectrometry. J Am Soc Mass Spectrom. 1999; 10:1124–1130. [PubMed: 10536818]
23. Korndörfer IP, Brueckner F, Skerra A. The crystal structure of the human $(S100A8/S100A9)_2$ heterotetramer, calprotectin, illustrates how conformational changes of interacting a-helices can determine specific association of two EF-hand proteins. J Mol Biol. 2007; 370:887–898. [PubMed: 17553524]
24. Santamaria-Kisiel L, Rintala-Dempsey AC, Shaw GS. Calcium-dependent and -independent interactions of the S100 protein family. Biochem J. 2006; 396:201–214. [PubMed: 16683912]
25. Gifford JL, Walsh MP, Vogel HJ. Structures and metal-ion-binding properties of the Ca^{2+}-binding helix–loop–helix EF-hand motifs. Biochem J. 2007; 405:199–221. [PubMed: 17590154]
26. Strupat K, Rogniaux H, Van Dorsselaer A, Roth J, Vogl T. Calcium-induced noncovalently linked tetramers of MRP8 and MRP14 are confirmed by electrospray ionization-mass analysis. J Am Soc Mass Spectrom. 2000; 11:780–788. [PubMed: 10976885]

27. Vogl T, Leukert N, Barczyk K, Strupat K, Roth J. Biophysical characterization of S100A8 and S100A9 in the absence and presence of bivalent cations. Biochim Biophys Acta. 2006; 1763:1298–1306. [PubMed: 17050004]
28. Stephan JR, Nolan EM. Calcium-induced tetramerization and zinc chelation shield human calprotectin from degradation by host and bacterial extracellular proteases. Chem Sci. 2016; 7:1962–1975. [PubMed: 26925211]
29. Irving I, Williams RJP. Irving Williams series. Nature. 1948; 162:746–747.
30. Grabarek Z. Structural Basis for Diversity of the EF-hand Calcium-binding Proteins. J Mol Biol. 2006; 359:509–525. [PubMed: 16678204]
31. Bertin EP. Introduction to X-Ray Spectrometric Analysis Springer US; Boston, MA: 1978 Energy-Dispersive X-Ray Spectrometry; 231253
32. Bowman SEJ, Bridwell-Rabb J, Drennan CL. Metalloprotein crystallography: more than a structure. Acc Chem Res. 2016; 49:695–702. [PubMed: 26975689]
33. Walkup GK, Burdette SC, Lippard SJ, Tsien RY. A new cell-permeable fluorescent probe for Zn^{2+} J Am Chem Soc. 2000; 122:5644–5645.
34. Cunden LS, Brophy MB, Rodriguez GE, Flaxman HA, Nolan EM. Biochemical and functional evaluation of the intramolecular disulfide bonds in the zinc-chelating antimicrobial protein human S100A7 (psoriasin). Biochemistry. 2017; 56:5726–5738. [PubMed: 28976190]
35. Cunden LS, Gaillard A, Nolan EM. Calcium ions tune the zinc-sequestering properties and antimicrobial activity of human S100A12. Chem Sci. 2016; 7:1338–1348. [PubMed: 26913170]
36. Berman HM, Westbrook J, Feng Z, Gilliland G, Bhat TN, Weissig H, Shindyalov IN, Bourne PE. The Protein Data Bank. Nucl Acids Res. 2000; 28:235–242. [PubMed: 10592235]
37. Hsin K, Sheng Y, Harding MM, Taylor P, Walkinshaw MD. MESPEUS: a database of the geometry of metal sites in proteins. J Appl Crystallogr. 2008; 41:963–968.
38. Weekes D, Miller MD, Krishna SS, McMullan D, McPhillips TM, Acosta C, Canaves JM, Elsliger MA, Floyd R, Grzechnik SK, Jaroszewski L, Klock HE, Koesema E, Kovarik JS, Kreusch A, Morse AT, Quijano K, Spraggon G, van den Bedem H, Wolf G, Hodgson KO, Wooley J, Deacon AM, Godzik A, Lesley SA, Wilson IA. Crystal structure of a transcription regulator (TM1602) from *Thermotoga maritima* at 2.3 Å resolution. Proteins: Struct, Funct Bioinf. 2007; 67:247–252.
39. Löw C, Neumann P, Tidow H, Weininger U, Haupt C, Friedrich-Epler B, Scholz C, Stubbs MT, Balbach J. Crystal structure determination and functional characterization of the metallochaperone SlyD from *Thermus thermophilus*. J Mol Biol. 2010; 398:375–390. [PubMed: 20230833]
40. Håkansson KO. The crystallographic structure of Na,K-ATPase N-domain at 2.6 Å resolution. J Mol Biol. 2003; 332:1175–1182. [PubMed: 14499619]
41. Salgado EN, Lewis RA, Mossin S, Rheingold AL, Tezcan FA. Control of protein oligomerization symmetry by metal coordination: C_2 and C_3 symmetrical assemblies through Cu^{II} and Ni^{II} coordination. Inorg Chem. 2009; 48:2726–2728. [PubMed: 19267481]
42. Santoro A, Mighell AD, Zocchi M, Reimann CW. The crystal and molecular structure of hexakis(imidazole)nickel(II) nitrate, $(C_3H_4N_2)_6Ni(NO_3)_2$. Acta Crystallogr Sect B: Struct Sci. 1969; 25:842–847.
43. Konopelski JP, Reimann CW, Hubbard CR, Mighell AD, Santoro A. Hexakis(imidazole)nickel(II) chloride tetrahydrate. Acta Crystallogr Sect B: Struct Sci. 1976; 32:2911–2913.
44. Donato R, Cannon BR, Sorci G, Riuzzi F, Hsu K, Weber DJ, Geczy CL. Functions of S100 proteins. Curr Mol Med. 2013; 13:24–57. [PubMed: 22834835]
45. Moroz OV, Burkitt W, Wittkowski H, He W, Ianoul A, Novitskaya V, Xie J, Polyakova O, Lednev IK, Shekhtman A, Derrick PJ, Bjoerk P, Foell D, Bronstein IB. Both Ca^{2+} and Zn^{2+} are essential for S100A12 protein oligomerization and function. BMC Biochem. 2009; 10:11. [PubMed: 19386136]
46. Baudier J, Glasser N, Gerard D. Ions binding to S100 proteins. I. Calcium- and zinc-binding properties of bovine brain S100aa, S100a (aβ), and S100b (ββ) protein: Zn^{2+} regulates Ca^{2+} binding on S100b protein. J Biol Chem. 1986; 261:8192–8203. [PubMed: 3722149]
47. Chaudhuri D, Horrocks WD, Amburgey JC, Weber DJ. Characterization of lanthanide ion binding to the EF-hand protein S100β by luminescence spectroscopy. Biochemistry. 1997; 36:9674–9680. [PubMed: 9245399]

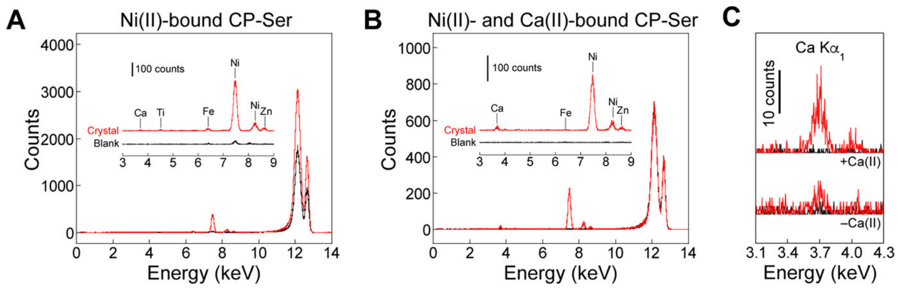

Figure 1.

EDX emission spectra of CP-Ser crystals. The metal content of each protein crystal was analyzed prior to X-ray diffraction data collection. (A) The Ni(II)-bound CP-Ser crystal contains Ni, Ca, and Zn as well as trace amounts of Ti and Fe. (B) The Ni(II)- and Ca(II)-bound CP-Ser crystal contains Ni and Zn as well as trace amounts of Ca and Fe. (C) Zoom on Ca Kα_1 region of both samples. Scans were obtained for the protein crystal (red line) and a blank sample (black line). Compton scatter is observed at the fixed incident energy at 0.9792 Å (12,622 eV). Peak positions indicated on the plots correspond to element K-edge transitions: Ca Kα_1 (3.69 keV), Ti Kα_1 (4.51 keV), Fe Kα_1 (6.40 keV), Ni Kα_1 (7.48 keV), Ni Kβ_1 (8.26 keV), and Zn Kα_1 (8.64 keV). We note that the magnitude of counts are different between the Ca(II)-free and Ca(II)-bound analyses. The ratio of Ca/Ni in the Ni(II)- and Ca(II)-bound CP-Ser is larger than the negligible ratio of Ca/Ni in the Ni(II)-bound CP-Ser. These data are hard to quantify because the Ca signal in the Ca-free crystal is just above the noise. Although the data collection time for each sample and its corresponding blank were identical, the collection time and thickness of crystals varied between sample/blank pairs, accounting for the differences in count magnitude observed.

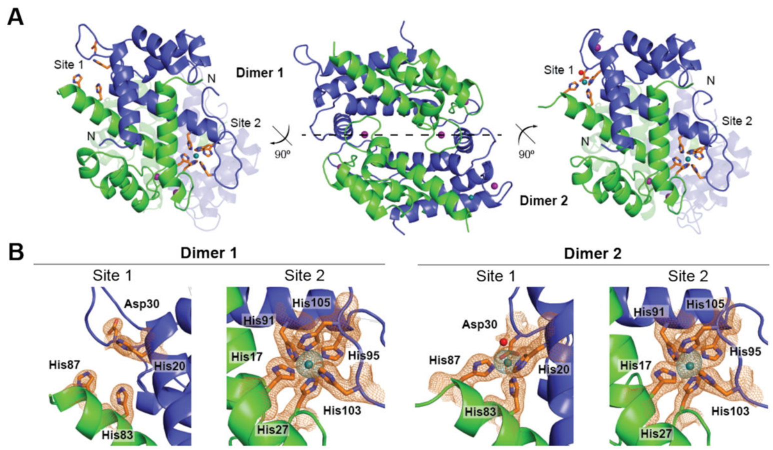

Figure 2.
Ni(II)-bound CP-Ser crystal structure. (A) CP-Ser forms an $\alpha_2\beta_2$ heterotetramer (middle) in the presence of Ni(II). The dashed line represents the dimer-dimer interface. The two heterodimers (left and right) are shown. The transition-metal-binding sites and the N-termini are labeled. The S100A8 subunits of both dimers 1 and 2 bind two Na(I) ions at the noncanonical and canonical EF-hand domains. The S100A9 subunit of dimer 2 binds one Na(I) ion at the noncanonical EF-hand domain. (B) Two transition-metal-binding sites form at the S100A8/S100A9 interface. The sites of each heterodimer are shown. Dimer 1 binds one Ni(II) at site 2, and dimer 2 binds two Ni(II) ions located at sites 1 and 2. The metal occupancy is summarized in Table 1. S100A8 is green, S100A9 is blue, Ni(II) ions are teal spheres, Na(I) ions are purple spheres, and water molecules are red spheres. A 2*Fo-Fc* composite omit electron density map (orange mesh) to 2.1-Å resolution is contoured at 1σ around the metal sites. A 2.3-Å resolution nickel anomalous difference map, calculated using data collected at a wavelength of 1.4831 Å, is contoured at 5σ and shown in teal.

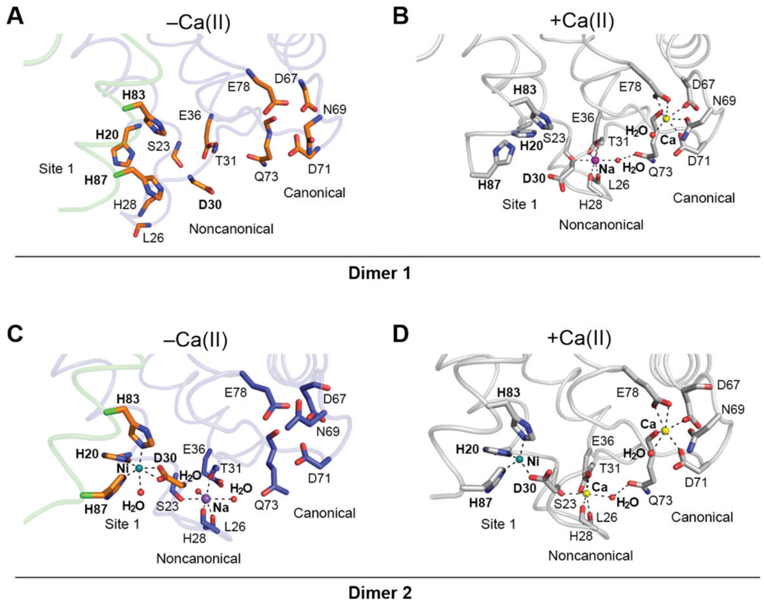

Figure 3.

Calcium-induced conformational changes near site 1. In these structural alignments, the metal-binding ligands of the EF-hands are shown (Table S7). (A and B) In dimer 1, Ca(II) binding at the canonical EF-hand domain of S100A9 results in conformational changes in the non-canonical domain and allows for (A9)Asp30 to be positioned to form the His_3Asp motif. The loop of the non-canonical EF-hand domain exhibits a relatively large conformational change. (C and D) Coordination of Ca(II) ions at both EF-hand domains results in a change in coordination number at the His_3Asp motif of dimer 2. In the Ca(II)-free structure, two water molecules coordinate the Na(I) ion at the S100A9 non-canonical EF-hand domain, whereas a bidentate Glu36 and one water molecule (with a hydrogen bond interaction with Gln73) coordinate Ca(II) in the Ca(II)-bound form. The Ca(II)-free structures (A and C) are depicted in color, where S100A8 is green and S100A9 is blue. The Ca(II)-bound structures (B and D) are in gray. The residues of site 1 and the EF-hand domains are in orange (−Ca(II)) or gray (+Ca(II)). Ni(II) ions are teal spheres. Na(I) ions are purple spheres. Ca(II) ions are yellow spheres. Water molecules are red spheres. Metal–ligand and hydrogen bonds are shown as dashed lines.

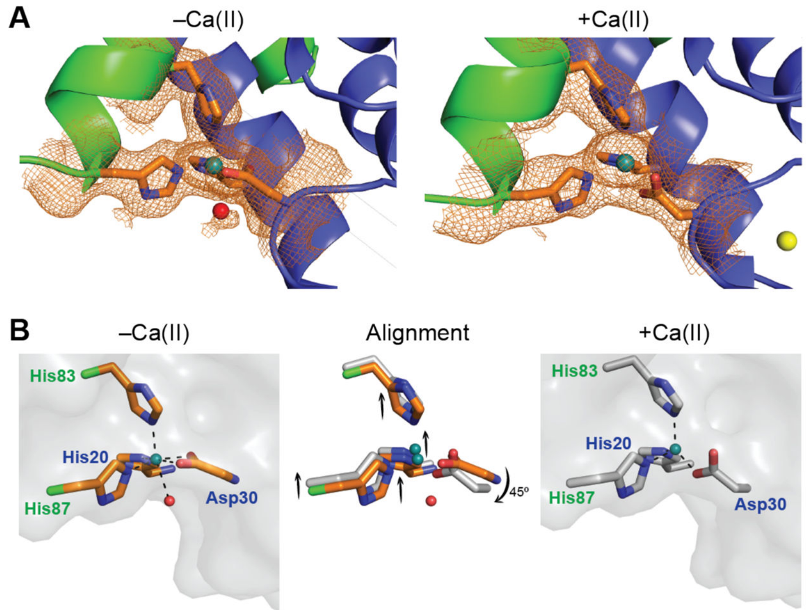

Figure 4.

Change in coordination number at the His_3Asp motif of dimer 2 with Ca(II) binding. (A) Electron density at site 1 of dimer 2 in the Ca(II)-free and Ca(II)-bound CP-Ser crystal structures. A 2*Fo-Fc* composite omit electron density map (orange mesh) to 2.1-Å (−Ca(II)) or 2.6-Å (+Ca(II)) resolution is contoured at 0.5σ around the His_3Asp motif. (B) The six-coordinate Ni(II) site of the Ca(II)-free structure is shown in color (left), and the four-coordinate Ni(II) site of the Ca(II)-bound structure is shown in gray (right). The metal-binding residues are depicted in orange (−Ca(II)) and gray (+Ca(II)). Space-filling models of the proteins are shown in gray. A structural alignment of all alpha carbons is depicted in the middle, and the conformational changes from Ca(II)-free to Ca(II)-bound are shown as arrows. S100A8 residues are labeled in green, and S100A9 residues are labeled in blue. Ni(II) ions are teal spheres. The water molecule is a red sphere. Metal–ligand bonds are shown as dashed lines.

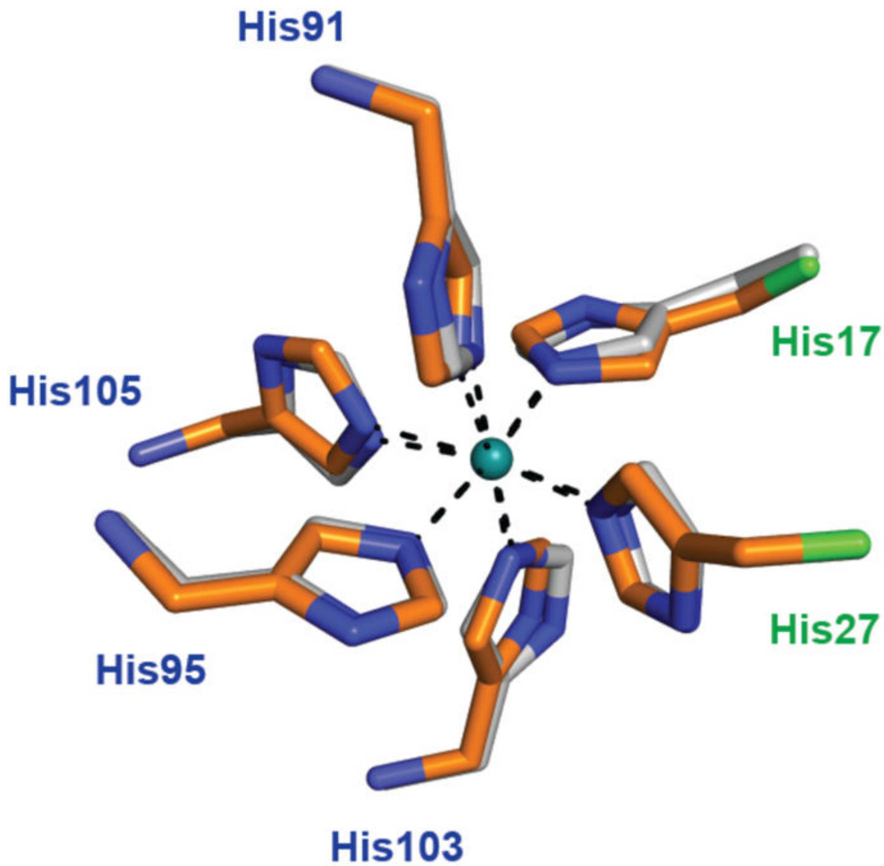

Figure 5.

Structural alignment of the Ni(II)-His_6 motif. The Ca(II)-free structure is depicted in color, and the Ca(II)-bound structure is in gray. S100A8 residues are labeled in green, and S100A9 residues are labeled in blue. The Ni(II) ion is depicted as a teal sphere. Models of site 2 of dimer 1 are shown. Further details of the structural alignment at site 2 are shown in Figure S2.

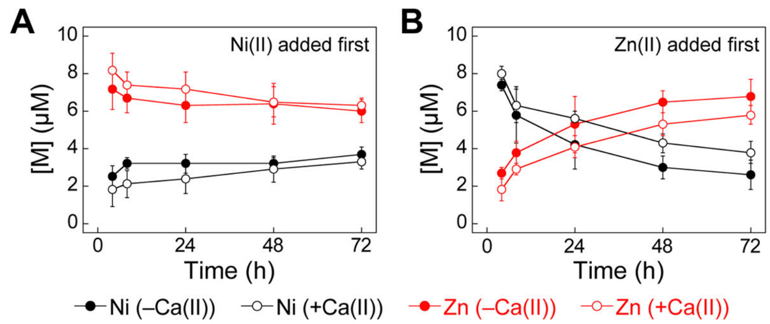

Figure 6.

Metal substitution of the His_6 site is slowed in the presence of Ca(II). Metal content of supernatant of B-ΔHis_3Asp (10 μM) incubated with 10 μM Ni(II) and Zn(II) in the absence and presence of 2 mM Ca(II) (room temperature; 75 mM HEPES, 100 mM NaCl, pH 7.0) after treatment with streptavidin agarose resin. (A) Zn(II) was added to a pre-equilibrated solution of Ni(II) and B-ΔHis_3Asp. (B) Ni(II) was added to a pre-equilibrated solution of Zn(II) and B- ΔHis_3Asp. The Ni (black) and Zn (red) concentrations were measured by ICP-MS. Closed circles represent metal content without Ca(II), and open circles represent metal content with Ca(II). The mean and SDM are reported (n = 4).

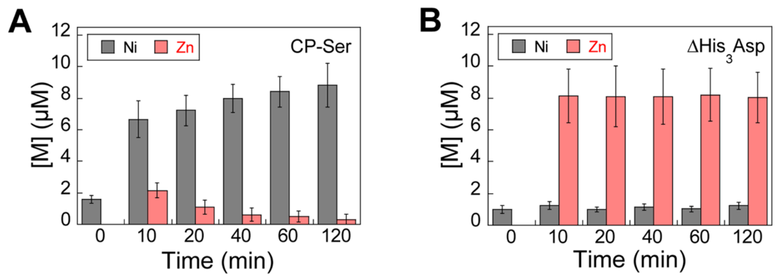

Figure 7.

Zn(II) rapidly displaces Ni(II) at the His_3Asp site in the presence of 2 mM Ca(II). (A) Metal content of filtrate of CP-Ser (10 μM) pre-incubated with 20 μM Ni(II) and supplemented with 10 μM Zn(II). (B) Metal content of filtrate of His_3Asp (10 μM) pre-incubated with 10 μM Ni(II) and supplemented with 10 μM Zn(II). All solutions of protein and metal contained 2 mM Ca(II) and were prepared in 75 mM HEPES, 100 mM NaCl, pH 7.0. Protein was incubated for 1 hour with Ni(II) before Zn(II) addition. The t = 0 h time point is the flow through before Zn(II) addition, and all subsequent times correspond to the time post-Zn(II) addition. The Ni (gray) and Zn (red) concentrations were measured by ICP-MS. The mean and SDM are reported ($n = 3$). Data obtained in the absence of 2 mM Ca(II) are presented in Figure S7.

Table 1

Nature of Metal Ions in Ni(II)-bound CP-Ser Crystal Structure[a]

Dimer	Subunit	N-EF [b c]	C-EF [c d]	His_3Asp [c e]	His_6 [e]
1	S100A8	Na	Na	–	Ni
	S100A9	–	–		
2	S100A8	Na	Na	Ni	Ni
	S100A9	Na	–		

[a] All metals were modeled at 100% occupancy.

[b] Noncanonical N-terminal EF-hand domain.

[c] Dashes denote binding sites without a metal atom modeled in.

[d] Canonical C-terminal EF-hand domain.

[e] Each S100A8/S100A9 dimer comprises two interfacial transition-metal-binding sites.